

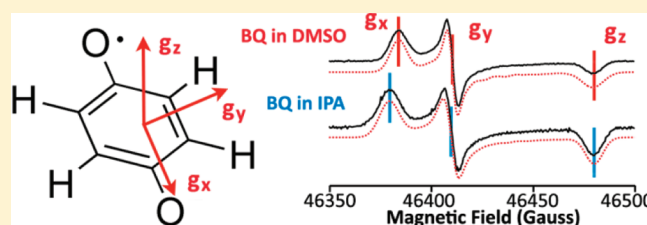
# Structure and Function of Quinones in Biological Solar Energy Transduction: A High-Frequency D-Band EPR Spectroscopy Study of Model Benzoquinones

Ruchira Chatterjee,<sup>†</sup> Christopher S. Coates,<sup>†</sup> Sergey Milikisiyants,<sup>†</sup> Oleg G. Poluektov,<sup>‡</sup> and K. V. Lakshmi<sup>\*,†</sup>

<sup>†</sup>Department of Chemistry and Chemical Biology and The Baruch '60 Center for Biochemical Solar Energy Research, Rensselaer Polytechnic Institute, Troy, New York 12180, United States

<sup>‡</sup>Chemical Sciences and Engineering Division, Argonne National Laboratory, 9700 South Cass Avenue, Argonne, Illinois 60439, United States

**ABSTRACT:** Quinones are utilized as charge-transfer cofactors in a wide variety of reactions that are crucial for photosynthesis and respiration. In photosynthetic protein complexes, both Type I and Type II, including oxygenic and anoxygenic reaction centers contain quinone cofactors that are known to participate in electron- and proton-transfer processes. Type II reaction centers, purple bacterial reaction centers, and photosystem II utilize benzoquinone molecules, ubiquinone, and plastoquinone, respectively, to facilitate proton-coupled electron transfer reactions. Here, we report a systematic study of the principal components of the *g*-tensor of an extensive library of model benzosemiquinone anion radicals in both protic (2-isopropanol) and aprotic (dimethyl sulfoxide) solvents using high-frequency EPR spectroscopy. A detailed comparison of the experimental *g*-values of the benzosemiquinone models at D-band EPR frequency allows for the discrimination of substituent effects and solvent hydrogen bonds on the principal components of the *g*-tensor. Further, we compare the primary plastosemiquinone,  $Q_A^-$ , of photosystem II with the substituent and solvent hydrogen bond effects of benzosemiquinone models *in vitro*. This study significantly extends the experimental basis for elucidating the role of both molecular structure and interactions with environment on the functional tuning of quinone cofactors in biological solar energy transduction.



## INTRODUCTION

Quinones are utilized as charge-transfer cofactors in a wide variety of reactions that are crucial for photosynthesis and respiration.<sup>1–10</sup> In photosynthetic protein complexes, both Type I and Type II, including oxygenic and anoxygenic reaction centers (RC), contain quinone cofactors that are known to participate in electron- and proton-transfer processes. While photosystem I (PSI) utilizes phyloquinone molecules for the transfer of reducing equivalents through the electron transport chain,<sup>9–11</sup> the bacterial RC (BRC) and photosystem II (PSII) utilize benzoquinone molecules to facilitate proton-coupled electron transfer reactions.<sup>1–8</sup> There are significant differences in the function of the quinones in different RCs. Thus, similar quinones can operate at up to 800 mV lower reduction potential when present in type I RCs.<sup>12–16</sup>

The versatility of quinones and the diversity of their biological function are controlled by both intra- and intermolecular interactions. The differences in the functional specificity of quinones is suggested to arise from the structure and location of the quinone cofactor, the geometry of its binding site and the smart matrix effects from the surrounding protein environment that greatly influence the charge-transfer properties of quinones.<sup>14</sup> Therefore, knowledge of electronic structure and its correlation with the chemical structure of the quinones as well as the interaction with the local protein environment is of importance in understanding the versatility of quinone function in biological

solar energy transduction. This is also significant for the potential application of quinones in the development of artificial photosynthetic systems for solar energy conversion.<sup>17–20</sup>

Electron paramagnetic resonance (EPR) spectroscopy is a powerful tool to study the electronic structure of paramagnetic species.<sup>21–29</sup> In particular, it is possible to resolve the electronic *g*-tensor of organic radical species at higher EPR frequency.<sup>24,30–32</sup> The EPR observables that are obtained from the analysis of high-frequency EPR (HF EPR) spectra, such as the *g*-tensor, are highly sensitive to subtle changes in the distribution of the electron spin density. In the case of the semiquinone anion radical, the *g*-tensor has been shown to depend not only on the chemical structure of the semiquinone but also on the interactions of the semiquinone with the surrounding matrix.<sup>33,34</sup> Thus, the electronic *g*-tensor is an important spectroscopic probe of the intra- and intermolecular interactions of semiquinone radicals.

In recent years, the *g*-tensor of semiquinone anion radicals both *in vivo*<sup>35,36</sup> and *in vitro*<sup>37–39</sup> has been an attractive subject of experimental and theoretical investigations.<sup>40–42</sup> Although the results obtained in these studies have demonstrated the application of HF EPR spectroscopy to investigate the interactions of semiquinone anion radicals,<sup>43</sup> such as hydrogen (H-) bonds to

**Received:** October 22, 2011

**Revised:** November 27, 2011

**Published:** December 14, 2011

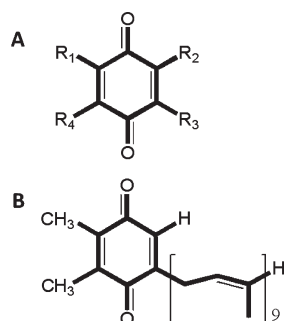


**Figure 1.** Chemical structure and substituent groups of (A) BQ:  $R_1 = R_2 = R_3 = R_4 = H$ . pPBQ:  $R_1 = \text{phenyl}$ ,  $R_2 = R_3 = R_4 = H$ . DPBQ:  $R_1 = R_3 = \text{phenyl}$ ,  $R_2 = R_4 = H$ . DMBQ:  $R_1 = R_3 = \text{methyl}$ ,  $R_2 = R_4 = H$ . TMBQ:  $R_1 = R_2 = R_3 = R_4 = \text{methyl}$ . DCBQ:  $R_1 = R_3 = \text{chloro}$ ,  $R_2 = R_4 = H$ . TCBQ:  $R_1 = R_2 = R_3 = R_4 = \text{chloro}$  and (B) plastoquinone, PQ.

the carbonyl keto oxygen atom(s) of the semiquinone and  $\pi$ -stacking interactions with the semiquinone ring, the specific role of these interactions in the functional tuning of quinones remains unknown. Further, the effect of H-bonds of model semiquinones in protic solvents has been previously investigated by HF EPR spectroscopy;<sup>44–46</sup> however, there exists a lack of comparative experimental data on the g-tensor of semiquinone radicals in an aprotic environment,<sup>47,48</sup> which hinders the development of theoretical models.

We report a systematic HF EPR spectroscopy study of the principal components of the g-tensor of an extensive library of model benzoquinone anion radicals in an aprotic (dimethyl sulfoxide; DMSO) and protic (2-isopropanol; IPA) solvent. In this study, the increased electron Zeeman interaction at D-band (130 GHz) microwave frequency leads to the complete resolution of spectral features arising from the three canonical orientations of the g-tensor of the benzoquinone models. A detailed comparison of the experimental g-values of the benzoquinone models allows for the isolation of substituent effects and solvent H-bonds on the principal components of the g-tensor. Further, comparison of the EPR properties of the primary plastoquinone,  $Q_A^-$ , of PSII with those of model benzoquinones in vitro provides a better understanding of the tuning and control of quinone cofactors in photosynthetic reaction centers.

## MATERIALS AND METHODS

**Preparation of Benzoquinone Anion Radicals.** The library of benzoquinone model compounds used in this study was obtained from commercial sources. 1,4-Benzoquinone (BQ) (98%), 2,5-dimethyl-1,4-benzoquinone (DMBQ) (99%), 2,3,5,6-tetramethyl-1,4-benzoquinone (TMBQ) (99%), and 2-phenyl-1,4-benzoquinone (pPBQ) (99%) were purchased from Acros Organics (Morris Plains, NJ). 2,3,5,6-Tetrachloro-1,4-benzoquinone (TCBQ) (99%) was purchased from Sigma-Aldrich (St. Louis, MO). 2,5-Dichloro-1,4-benzoquinone (DCBQ) (98%) and 2,5-diphenyl-1,4-benzoquinone (DPBQ) (99%) were purchased from Pfaltz & Bauer (Waterbury, CT) (Figure 1). The benzoquinone anion radicals were generated by dissolving the quinone (1 mM to 10 mM) in dimethyl sulfoxide (DMSO) or isopropyl alcohol (IPA), and the solution was purged with dry nitrogen gas. To this mixture, a reducing agent, either 10 M aqueous sodium hydroxide (to DMSO) or a minimum amount

of potassium tertiary-butoxide solution (to IPA), was added dropwise under an inert nitrogen gas atmosphere.<sup>49</sup> The benzoquinone in solution was loaded into 0.3 mm (inner diameter) quartz capillary tubes (VitroCon, Mountain Lakes, NJ), and the sample was rapidly frozen at liquid helium temperature (32 K) within the EPR resonator for the D-band HF EPR spectroscopy measurements.

**Growth and Isolation of Histidine-Tagged Photosystem II Complexes from the PsbB Variant of *Synechocystis* PCC 6803.** The hexa-histidine-tagged (HT) PsbB variant of *Synechocystis* PCC 6803 was prepared by minor modification of previously published procedures.<sup>50</sup> The PsbB variant of *Synechocystis* PCC 6803 was grown on agar plates containing BG-11 medium (1.76 M sodium nitrate ( $\text{NaNO}_3$ ), 30.3 mM magnesium sulfate ( $\text{MgSO}_4$ ), 24.5 mM calcium chloride ( $\text{CaCl}_2$ ), 3.14 mM citric acid and a mixture containing boric acid ( $\text{H}_3\text{BO}_3$ ), manganese chloride ( $\text{MnCl}_2$ ), zinc sulfate ( $\text{ZnSO}_4$ ), molybdic acid ( $\text{H}_2\text{MoO}_4$ ), cupric sulfate ( $\text{CuSO}_4$ ), and cobalt nitrate ( $\text{Co}(\text{NO}_3)_2$ ).<sup>51</sup> The single colonies of the PsbB variant of *Synechocystis* PCC 6803 were harvested from the BG-11 agar plates, subcultured to 100 mL growths and propagated to 18 L liquid cultures under constant illumination at  $\sim 30^\circ\text{C}$  using liquid BG-11 medium with 5 mM glucose and 5 mM 2-[[1,3-dihydroxy-2-(hydroxymethyl)propan-2-yl]amino]ethanesulfonic acid/potassium hydroxide ((TES)-KOH) at pH 8.2.<sup>51</sup> The cells were harvested by continuous-flow filtration (Millipore, Billerica, MA) and resuspended in buffer containing 50 mM 2-(N-morpholino)ethanesulfonic acid/sodium hydroxide (MES-NaOH) at pH 6.0, 5 mM  $\text{CaCl}_2$ , 5 mM magnesium chloride ( $\text{MgCl}_2$ ), and 25% w/v glycerol. The cells were broken using a bead-beater (BioSpec, Bartlesville, OK), and the thylakoids were separated by ultracentrifugation. The thylakoids were used to prepare a detergent (dodecyl- $\beta$ -D-maltoside) ( $\beta$ -DM)-solubilized extract of proteins in buffer containing 50 mM MES-NaOH, pH 6.0, 20 mM  $\text{CaCl}_2$ , 5 mM  $\text{MgCl}_2$ , 25% (w/v) glycerol, and 0.03% (w/v)  $\beta$ -DM. The protein extract was subjected to purification on a  $\text{Ni}^{2+}$ -metal affinity chromatography column (Qiagen, Valencia, CA) to isolate pure HT-PSII complexes.<sup>50</sup> The isolation and purification procedures were conducted in the dark at  $4^\circ\text{C}$ . The resulting PSII complexes were monitored by SDS-PAGE analysis.

The HT-PSII complexes were manganese (Mn)-depleted in buffer containing 50 mM MES-NaOH, pH 6.0, 20 mM  $\text{CaCl}_2$ , 5 mM  $\text{MgCl}_2$ , 25% w/v glycerol, 0.03% w/v  $\beta$ -DM, 10 mM hydroxylamine hydrochloride ( $\text{NH}_2\text{OH}\cdot\text{HCl}$ ), and 10 mM sodium ethylenediamine tetraacetic acid (Na-EDTA).<sup>52</sup> The Mn-depleted HT-PSII was washed in a buffer containing 50 mM MES-NaOH, pH 6.0, 20 mM  $\text{CaCl}_2$ , 5 mM  $\text{MgCl}_2$ , 25% w/v glycerol, 0.03% w/v  $\beta$ -DM, and 5 mM Na-EDTA. The high-spin (electron spin  $S = 2$ ) nonheme iron center, Fe(II), in Mn-depleted HT-PSII was converted to its low-spin (electron spin  $S = 0$ ) state by incubating with 350 mM potassium cyanide (KCN) at pH 6.5 for 3.5 h in the dark at  $4^\circ\text{C}$ .<sup>53</sup> The Mn-depleted, CN-treated HT-PSII was suspended in a deuterated glycine buffer at pH 10.02, where deuterated water ( $\text{D}_2\text{O}$ ) was used in place of  $\text{H}_2\text{O}$  in the buffer. After repeated freeze–pump–thaw cycles, the Mn-depleted, CN-treated HT-PSII in deuterated buffer was treated with sodium dithionite to chemically reduce the neutral primary plastoquinone,  $Q_A$ , to the reduced plastoquinone state,  $Q_A^-$ . The Mn-depleted, CN-treated HT-PSII with the reduced  $Q_A^-$  semiquinone state was used for the D-band (130 GHz) HF EPR spectroscopy measurements.

**High-Frequency D-Band EPR Spectroscopy.** The HF EPR spectra were recorded on a home-built D-band (130 GHz)

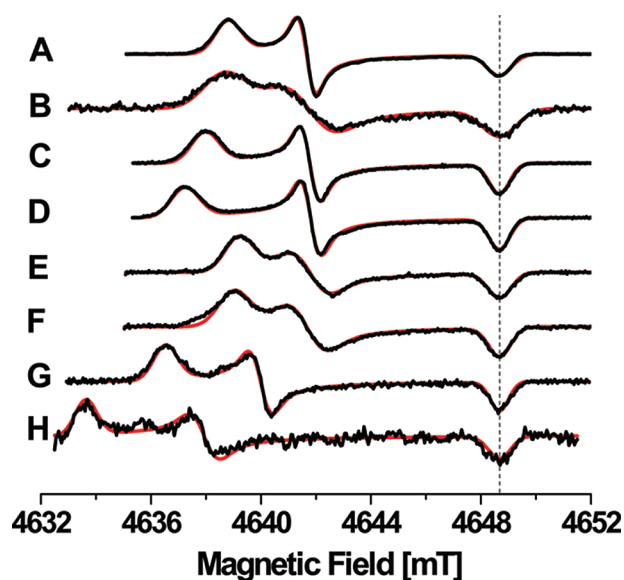


**Figure 2.** First derivative of the spin-echo-detected field-sweep D-band (130 GHz) EPR spectrum of model benzoquinone anion radicals with DMSO as the solvent. (A) 1,4-benzoquinone (BQ), (B) plastoquinone-9 (PQ), (C) 2-phenyl-1,4-benzoquinone (pPBQ), (D) 2,5-diphenyl-1,4-benzoquinone (DPBQ), (E) 2,5-dimethyl-1,4-benzoquinone (DMBQ), (F) 2,3,5,6-tetramethyl-1,4-benzoquinone (TMBQ), (G) 2,5-dichloro-1,4-benzoquinone (DCBQ), and (H) 2,3,5,6-tetrachloro-1,4-benzoquinone (TCBQ). The experimental and simulated spectra are shown as black and red traces, respectively.

pulsed spectrometer described previously.<sup>31,54</sup> The HF EPR spectroscopy measurements were performed at 32 K. The temperature of the EPR sample was regulated by an Oxford ITC 503 temperature controller with an Oxford CF 1200 continuous-flow helium cryostat (Oxford Instruments, Oxfordshire, UK). The spin-echo-detected field-sweep HF EPR spectra were obtained using microwave pulses of 90 and 120 ns duration with a separation of 250 ns and a repetition rate of 40 Hz. The HF EPR spectra were processed using the software program SpecLab, and the numerical first derivative of the spin-echo-detected HF EPR spectra were simulated using the software program, SimBud (kindly provided by Dr. Astashkin at the Electron Paramagnetic Resonance Facility, Department of Chemistry, University of Arizona, Tucson, AZ). For the spectral simulations, the anisotropic  $g$ -tensor was used to reproduce the spectral features that are observed in the experimental EPR spectra. Other magnetic interactions that are much smaller in magnitude and hence unresolved in the HF EPR spectra (e.g., the electron-nuclear hyperfine interactions) were approximated by the intrinsic spectral line width that was assumed as a Gaussian function. In the present study, the relative  $g$ -values are measured with high precision ( $\sim 10^{-4}$ ). However, the absolute  $g$ -values could include systematic errors due to difficulty in the determination of the precise static magnetic field experienced by the EPR sample. As a reference, the value of the  $z$ -component of the  $g$ -tensor,  $g_z$ , was set to the  $g$ -value of a free electron,  $g = 2.00232$ . This is a valid approximation as the deviations of the  $g_z$  component are usually on the order of  $10^{-5}$ , which is much smaller than the variation of the values of the  $g_x$  and  $g_y$  components that are observed in this study ( $\sim 10^{-3}$ ).<sup>39</sup> The experimental and simulated HF EPR spectra that are presented here were prepared in Matlab R2008a.

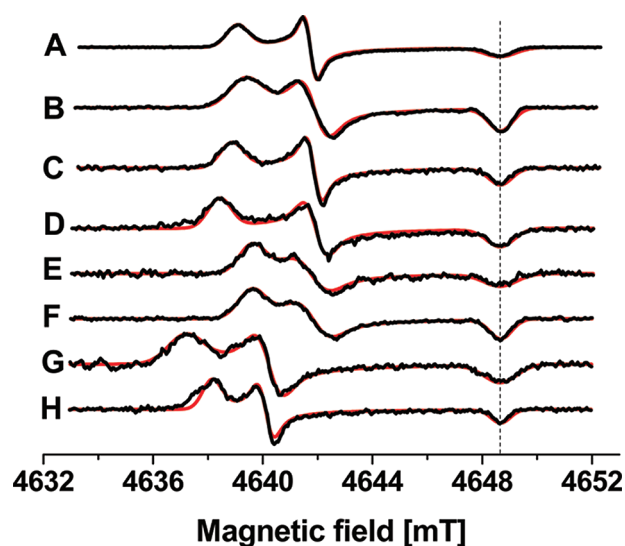


**Figure 3.** First derivative of the spin-echo-detected field-sweep D-band (130 GHz) EPR spectrum of model benzoquinone anion radicals with IPA as the solvent. (A) 1,4-benzoquinone (BQ), (B) plastoquinone-9 (PQ), (C) 2-phenyl-1,4-benzoquinone (pPBQ), (D) 2,5-diphenyl-1,4-benzoquinone (DPBQ), (E) 2,5-dimethyl-1,4-benzoquinone (DMBQ), (F) 2,3,5,6-tetramethyl-1,4-benzoquinone (TMBQ), (G) 2,5-dichloro-1,4-benzoquinone (DCBQ), and (H) 2,3,5,6-tetrachloro-1,4-benzoquinone (TCBQ). The experimental and simulated spectra are shown as black and red traces, respectively.

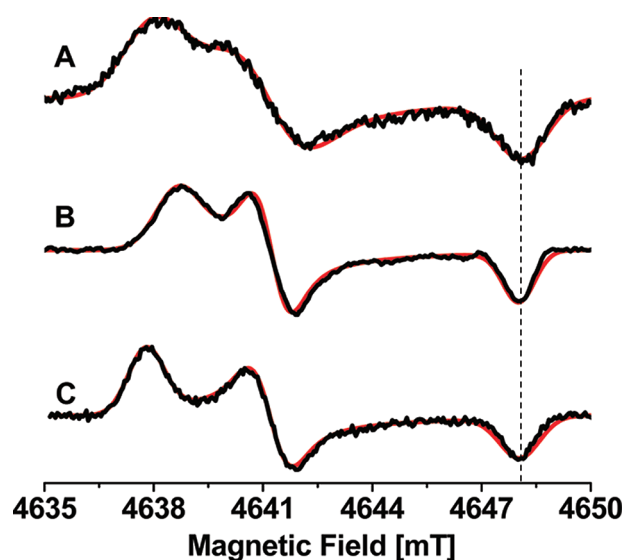


**Figure 4.** First derivative of the spin-echo-detected field-sweep D-band (130 GHz) EPR spectrum of (A) the plastoquinone anion radical in DMSO, (B) the plastoquinone anion radical in IPA, and (C) the plastoquinone anion radical of PSII,  $Q_A^-$ , in aqueous buffer. The experimental and simulated spectra are shown as black and red traces, respectively.

When recorded at conventional X-band microwave frequency (9–10 GHz), the spin-echo-detected EPR spectra are often distorted due to the presence of pronounced nuclear modulations when the anisotropy of the electron-nuclear hyperfine interaction is on the same order of magnitude as the nuclear Zeeman interaction. In the present study, the hyperfine interaction

**Table 1. Principal Components of the  $g$ -Tensor of the Model Benzosemiquinones Obtained from Spectral Line Shape Simulations of the Experimental HF D-band (130 GHz) EPR Spectra in DMSO and IPA, Respectively, and the Plastosemiquinone Anion,  $Q_A^-$ , of PSII**

semiquinone (abbreviation)	simulation parameters in DMSO <sup>a</sup>			simulation parameters in IPA <sup>a</sup>		
	$g_x$	$g_y$	$g_z$	$g_x$	$g_y$	$g_z$
1,4-benzoquinone (BQ)	2.00659	2.00535	2.00232	2.00647	2.005315	2.00232
plastoquinone-9 (PQ)	2.00665	2.00530	2.00232	2.00635	2.00525	2.00232
2-phenyl-1,4-benzoquinone (pPBQ)	2.00695	2.005295	2.00232	2.00656	2.00526	2.00232
2,5-diphenyl-1,4-benzoquinone (DPBQ)	2.007265	2.005286	2.00232	2.00675	2.00523	2.00232
2,5-dimethyl-1,4-benzoquinone (DMBQ)	2.00641	2.00528	2.00232	2.00623	2.00529	2.00232
2,3,5,6-tetramethyl-1,4-benzoquinone (TMBQ)	2.006495	2.00533	2.00232	2.00624	2.00526	2.00232
2,5-dichloro-1,4-benzoquinone (DCBQ)	2.00757	2.00697	2.00232	2.007295	2.00597	2.00232
2,3,5,6-tetrachloro-1,4-benzoquinone (TCBQ)	2.00882	2.00695	2.00232	2.00687	2.00602	2.00232
$Q_A^-$ in PSII (aqueous buffer)	2.00675	2.00527	2.00232			
	(aqueous buffer)	(aqueous buffer)	(aqueous buffer)			

<sup>a</sup>The principal values of the  $g$ -tensor are assigned in the following order:  $g_x > g_y > g_z$ .<sup>39</sup>

**Table 2. Effective  $g$ -Tensor,  $\Delta g_x$ , with the Corresponding Redox Potentials of Model Benzosemiquinones<sup>a</sup>**

semiquinone (abbreviation)	$\Delta g_x$ in DMSO	$\Delta g_x$ in IPA	redox potential (V)
1,4-benzoquinone (BQ)	0.00427	0.00415	-0.043 <sup>b</sup>
plastoquinone-9 (PQ)	0.00433	0.00403	-0.351 <sup>b</sup>
2-phenyl-1,4-benzoquinone (pPBQ)	0.00463	0.00424	-0.034 <sup>b</sup>
2,5-diphenyl-1,4-benzoquinone (DPBQ)	0.00494	0.00443	-0.025 <sup>b</sup>
2,5-dimethyl-1,4-benzoquinone (DMBQ)	0.00409	0.00391	-0.210 <sup>b</sup>
2,3,5,6-tetramethyl-1,4-benzoquinone (TMBQ)	0.00418	0.00392	-0.385 <sup>b</sup>
2,5-dichloro-1,4-benzoquinone (DCBQ)	0.00525	0.00498	0.227 <sup>b</sup>
2,3,5,6-tetrachloro-1,4-benzoquinone (TCBQ)	0.00650	0.00455	0.476 <sup>b</sup>
$Q_A^-$ in PSII (aqueous buffer)	0.00443 (aqueous buffer)	N/A	-0.148 <sup>c</sup>

<sup>a</sup>The redox potentials were measured in acetonitrile, and the values were referenced to ferrocene.<sup>50</sup> <sup>b</sup>From Weyers et al.<sup>50</sup> <sup>c</sup>From Ishikita and Knapp.<sup>61</sup>

of the benzosemiquinone anion radicals is typically in the range of  $\sim 10$ – $20$  MHz,<sup>39,49</sup> which is much smaller than the nuclear Zeeman interaction which is approximately 200 MHz at 130 GHz EPR frequency. This results in the complete suppression of nuclear modulations as is indeed confirmed in this study.

## RESULTS

Shown in Figures 2A–H are the D-band experimental (black trace) and simulated (red trace) first-derivative spin-echo-detected magnetic field-sweep EPR spectra of frozen solutions of the model benzosemiquinone anion radicals, 1,4-benzoquinone (BQ), plastoquinone-9 (PQ), 2-phenyl-1,4-benzoquinone (pPBQ), 2,5-diphenyl-1,4-benzoquinone (DPBQ), 2,5-dimethyl-1,4-benzoquinone (DMBQ), 2,3,5,6-tetramethyl-1,4-benzoquinone (TMBQ), 2,5-dichloro-1,4-benzoquinone (DCBQ), and 2,3,5,6-tetrachloro-1,4-benzoquinone (TCBQ), in the aprotic solvent, DMSO. The investigation of the semiquinone anion radicals at D-band EPR frequency, which is more than an order of magnitude higher than the conventional X-band EPR frequency, leads to enhanced resolution of the spectral features from the three principal components of the  $g$ -tensor. This is due to the increase in the resolution of the  $g$ -factor at higher magnetic field. As can be seen from the spectra shown in Figure 2A–H, the principal components of the  $g$ -tensor of the model benzosemiquinone

anion radicals in DMSO are well-resolved at D-band EPR frequency. Qualitative examination of the experimental HF EPR spectra (black traces) that are displayed in Figure 2 reveals that the  $g_x$  and  $g_y$  components of the  $g$ -tensor of the benzosemiquinone models depend on the substituent group(s) on the benzosemiquinone ring. Additional effects due to H-bonding interactions with the surrounding matrix are absent in these spectra as DMSO is an aprotic solvent.

Shown in Figures 3A–H are the D-band experimental (black trace) and simulated (red trace) first-derivative spin-echo-detected magnetic field-sweep EPR spectra of a frozen solution of model benzosemiquinone anion radicals (described above in Figure 2) in the protic solvent, IPA. As can be seen from the spectra shown in Figure 3A–H, the principal components of the  $g$ -tensor of the benzosemiquinone anion radicals in IPA are also well-resolved at D-band EPR frequency. Further, comparison of the  $g$ -tensors of the model benzosemiquinone anion radicals in DMSO and IPA indicates that in addition to substituent effects, the  $g$ -tensor of the model benzosemiquinone anion radicals in IPA is affected by interactions with the solvent. In Figure 3, the  $g_x$  and  $g_y$  components of the  $g$ -tensor display pronounced influence of the presence of H-bonds of the benzosemiquinone radicals with IPA.

Figure 4A–C displays the experimental (black trace) and simulated (red trace) D-band EPR spin-echo-detected magnetic field-sweep EPR spectra of the primary plastosemiquinone anion,

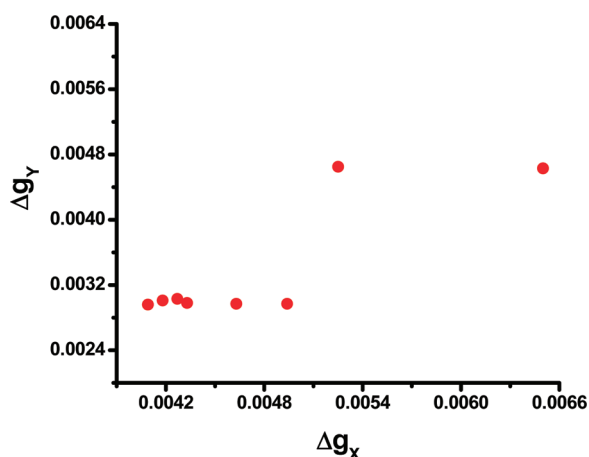


**Figure 5.** Correlation of the effective  $g$ -component of the  $g$ -tensor,  $\Delta g_x$  and  $\Delta g_y$ , of the model benzoquinones in DMSO.

$Q_A^-$ , of Mn-depleted, CN-treated PSII and the plastoquinone anion radical in IPA and DMSO, respectively. Once again, as can be seen in Figure 4A–C, the three principal components of the  $g$ -tensor of the plastoquinone anion radical both in vivo (Mn-depleted, CN-treated PSII) and in vitro (IPA and DMSO) are completely resolved at D-band EPR frequency.

The experimental spin-echo-detected magnetic field-sweep EPR spectra (black traces) in Figures 2–4 can be accurately reproduced by numerical simulations (red traces). The corresponding principal values of the  $g$ -tensor that are obtained from spectral simulations of the EPR spectra of the benzoquinone anion radicals are summarized in Table 1.

## DISCUSSION

The increased electron Zeeman interaction at D-band (130 GHz) EPR frequency leads to resolution of the  $g$ -tensor of the benzoquinone anion radical. In this study, through spectral simulations of the experimental HF EPR spectra, we compile the principal components of the  $g$ -tensor of an extensive library of model benzoquinones and the primary plastoquinone,  $Q_A^-$ , of PSII (Table 1). Listed in Table 2 is the effective  $g_x$  component of the  $g$ -tensor,  $\Delta g_x$ , with the corresponding redox potential of the benzoquinones. As can be seen in Table 2 and Figure 5, there is a clear relationship between the value of  $\Delta g_x$  in the aprotic solvent, DMSO, and the nature of the substituents that are present on the benzoquinone. A similar trend is also observed in the protic solvent, IPA (Table 2). The effective  $g_x$  component of the  $g$ -tensor,  $\Delta g_x$ , also displays a dependence on the redox potential of the benzoquinone. As can be seen in Table 2 and Figure 6, there is an increase in  $\Delta g_x$  with an increase (to a more positive value) of the redox potential of the corresponding benzoquinone.

The dependence of  $\Delta g$  on the nature of the substituents can be interpreted on the basis of the  $g$ -factor theory previously published by Stone.<sup>55</sup> Within a simplified Stone's theory, the deviation of the principal components of the  $g$ -tensor (Figure 7) from the free electron  $g$ -value for the benzoquinone anion radical, where the  $g$ -anisotropy originates from the excitation of an electron in a nonbonding lone-pair orbital on the keto oxygen atom to the half-occupied  $\pi$  orbital, can be expressed as<sup>39</sup>

$$\Delta g_x = \frac{2\xi\rho_0^\pi C_y^2}{\Delta E_{n\pi^*}} \quad (1)$$

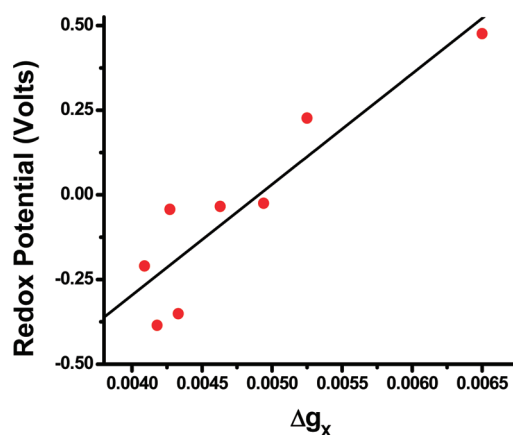


**Figure 6.** Correlation between the effective  $g_x$  component of the  $g$ -tensor,  $\Delta g_x$ , in DMSO and the redox potential of the corresponding model benzoquinones.

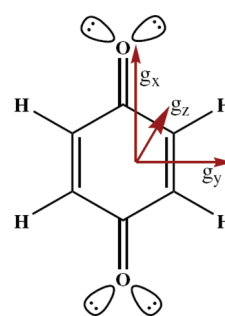


**Figure 7.** Orientation of the principal components of the  $g$ -tensor with respect to the molecular plane of the benzoquinone ring.

$$\Delta g_y = \frac{2\xi\rho_0^\pi C_x^2}{\Delta E_{n\pi^*}} \quad (2)$$

where  $\xi$  is the spin-orbit coupling parameter,  $\rho_0^\pi$  is the spin density of the  $\pi$  orbital on the oxygen atom, and  $C_x$  and  $C_y$  determine the admixtures of the  $p_x$  and  $p_y$  orbitals in the lone-pair orbitals of oxygen atom, respectively.  $\Delta E_{n\pi^*}$  is the difference in energy between the lone-pair orbitals and the half-occupied  $\pi$  orbital of the benzoquinone. As described by Burghaus and co-workers, a higher value of  $C_y$  explains the higher susceptibility of the value of the  $g_x$  component of the  $g$ -tensor to the presence of substituent groups on the benzoquinone ring.<sup>39</sup> Similarly,  $g_x$  would also have higher susceptibility to the polarity of the solvent.

Further examination of the  $g$ -tensors in Table 2 and Figure 5 reveals that the presence of a methyl group substituent reduces the  $g$ -anisotropy,  $\Delta g_x$ , of the benzoquinone. This is because a methyl group is electron donating in nature. This leads to a reduction of the electron spin density on the oxygen atom(s) through hyperconjugation effects.<sup>39,56,57</sup> However, this effect is clearly not additive with respect to the number of methyl groups that are present on the benzoquinone. This could be due to the presence of steric interaction between the multiple methyl groups on the ring. Similarly, the presence of a phenyl group leads to a larger  $\Delta g_x$  and this effect is enhanced with a larger number of phenyl group substituents. This is possibly due to the

dual nature of the phenyl group substituent that is electron-withdrawing based on resonance effects and is electron-donating through inductive effects. This could lead to an overall increase in the electron spin density on the oxygen atom(s) of the benzo-semiquinone.

There are large differences in  $\Delta g_x$  and  $\Delta g_y$  values that are observed in the presence of halogen groups, such as chloro-substituted benzosemiquinones (Table 2 and Figure 5).<sup>58,59</sup> This is in agreement with Stone theory as a chloro group has a larger spin-orbit coupling constant ( $\xi = 587 \text{ cm}^{-1}$ ).<sup>59</sup> It has been suggested that the positive shift of the  $g_x$  and  $g_y$  components is due to the participation of the chlorine  $p_z$  orbitals in the delocalized molecular  $\pi$  orbital of the benzosemiquinone ring.<sup>58</sup> Further, the electron-withdrawing nature of the chloro group also decreases the overall electron spin density distribution across the benzosemiquinone. This results in an increase of the electron spin density on the oxygen atom(s).

On the basis of the Stone theory, it is expected that H-bond interactions at the carbonyl oxygen atom(s) of the benzosemiquinone would influence  $\Delta g_x$  and could serve as direct probe of H-bond interactions. As can be seen in Table 2, the H-bond interaction of the benzosemiquinone in the protic solvent, IPA, reduces the value of  $\Delta g_x$ . It has been suggested by Burghaus and co-workers that the reduction of  $\Delta g_x$  upon increase in the electron spin density of the  $\pi$  orbital,  $\rho_0^\pi$ , can be attributed to the increase of the polarity of the C–O bond in the presence of a positively charged H atom and a lowering of the energy of the lone-pair orbital,  $E_{n\pi^*}$ , due to the formation of a bond between the orbital of the oxygen lone pair and the 1s orbital of the H-bonded atom leading to the subsequent increase of the energy gap in eqs 1 and 2.<sup>39</sup> These effects lead to the lowering of the value of  $g_x$  as the lone pair orbital is closely directed along the  $y$  axis (as opposed to the  $x$  axis). The  $g$ -tensor values obtained here are in good agreement with previous studies in literature.<sup>39</sup>

Finally, we compare the  $g$ -tensor of the plastosemiquinone in vivo,  $Q_A^-$  of PSII, with the  $g$ -tensor of the plastosemiquinone in vitro (Table 2). As can be seen, there is an increase in  $\Delta g_x$  when the plastosemiquinone is closely interacting with the surrounding protein environment of PSII. This is a direct consequence of the difference in the nature of the H-bond interactions in vivo and in vitro. In vitro, we observe highly symmetric H-bonds formed between the semiquinone radical and the protic solvent. However, it is known from previous studies that the  $Q_A^-$  anion has asymmetric H-bonds in vivo.<sup>60</sup> The  $g$ -tensor of  $Q_A^-$  in this study is in excellent agreement with the previously published literature.<sup>35</sup>

## SUMMARY

The experimental and theoretical reports on the  $g$ -tensors of various semiquinone species that have been published in recent years have dramatically improved the connection between the electronic structure, chemical structure,<sup>56,57</sup> and specific solute–solvent interactions.<sup>41,47,57</sup> However, the determinants of the functional tuning and control of quinone cofactors in biological solar energy transduction still remain unknown. The results of this study significantly extend the existing experimental database of the  $g$ -tensors of benzosemiquinone models in both protic and aprotic solvents. This facilitates comparison of the effects of molecular structure and interactions from the surrounding matrix on the electronic structure of benzosemiquinone anion radicals in vitro and within a protein environment.

## AUTHOR INFORMATION

### Corresponding Author

\*Phone: (518) 276 3271. Fax: (518) 276 4887. E-mail: lakshk@rpi.edu.

## ACKNOWLEDGMENT

We thank Dr. Andrei Astashkin (Electron Paramagnetic Resonance Facility, Department of Chemistry, University of Arizona, Tucson, AZ) for providing the spectral processing software, SpecLab, and the EPR spectral simulation program, SimBud. We also thank Amanda Weyers for assistance with sample preparation. This work was supported by the Division of Chemical Sciences, Geosciences, and Biosciences, Office of Basic Energy Sciences of the U.S. Department of Energy through Grants DE-FG02-07ER15903 (to K.V.L.) and DE-AC02-06CH11357 (to O.G.P.).

## ABBREVIATIONS

EPR	electron paramagnetic resonance spectroscopy
HF EPR	high-frequency EPR spectroscopy
RC	photosynthetic reaction center
BRC	bacterial reaction center
PSI	photosystem I
PSII	photosystem II
BQ	benzoquinone
H-bond	hydrogen bond

## REFERENCES

- (1) Lancaster, C. R. D.; Michel, H. *J. Mol. Biol.* **1999**, *286*, 883–898.
- (2) Allen, J. P.; Feher, G.; Yeates, T. O.; Rees, D. C.; Deisenhofer, J.; Michel, H.; Huber, R. *Proc. Natl. Acad. Sci. U.S.A.* **1986**, *83*, 8589–8593.
- (3) Feher, G.; Allen, J. P.; Okamura, M. Y.; Rees, D. C. *Nature* **1989**, *339*, 111–116.
- (4) Deisenhofer, J.; Epp, O.; Miki, K.; Huber, R.; Michel, H. *Nature* **1985**, *318*, 618–624.
- (5) Zouni, A.; Witt, H. T.; Kern, J.; Fromme, P.; Krauss, N.; Saenger, W.; Orth, P. *Nature* **2001**, *409*, 739–743.
- (6) Kamiya, N.; Shen, J. R. *Proc. Natl. Acad. Sci. U.S.A.* **2003**, *100*, 98–103.
- (7) Ferreira, K. N.; Iverson, T. M.; Maghlaoui, K.; Barber, J.; Iwata, S. *Science* **2004**, *303*, 1831–1838.
- (8) Loll, B.; Kern, J.; Saenger, W.; Zouni, A.; Biesiadka, J. *Nature* **2005**, *438*, 1040–1044.
- (9) Krauss, N.; Schubert, W. D.; Klukas, O.; Fromme, P.; Witt, H. T.; Saenger, W. *Nat. Struct. Biol.* **1996**, *3*, 965.
- (10) Jordan, P.; Fromme, P.; Witt, H. T.; Klukas, O.; Saenger, W.; Krauss, N. *Nature* **2001**, *411*, 909–917.
- (11) Golbeck, J. H. *Annu. Rev. Biophys. Biomol. Struct.* **2003**, *32*, 237–256.
- (12) Brettel, K.; Leibl, W. *Biochim. Biophys. Acta., Bioenerg.* **2001**, *1507*, 100–114.
- (13) Ptushenko, V. V.; Cherepanov, D. A.; Krishtalik, L. I.; Semenov, A. Y. *Photosyn. Res* **2008**, *97*, 55–74.
- (14) Srinivasan, N.; Golbeck, J. H. *Biochim. Biophys. Acta, Bioenerg.* **2009**, *1787*, 1057–1088.
- (15) Ishikita, H.; Knapp, E. W. *Biochemistry* **2005**, *44*, 14772–14783.
- (16) Ishikita, H.; Knapp, E. W. *J. Biol. Chem.* **2003**, *278*, 52002–52011.
- (17) Gust, D.; Moore, T. A.; Moore, A. L. *Acc. Chem. Res.* **1993**, *26*, 198–205.
- (18) Gust, D.; Moore, T. A. *Top. Curr. Chem.* **1991**, *159*, 103–151.
- (19) Moore, T. A.; Gust, D.; Mathis, P.; Mialocq, J. C.; Chachat, C.; Bensasson, R. V.; Land, E. J.; Doizi, D.; Liddell, P. A.; Lehman, W. R. et al. *Nature* **1984**, *307*, 630–632.

- (20) Moore, T. A.; Moore, A. L.; Gust, D. *Philos. Trans. R. Soc. London, Ser. B* **2002**, 357, 1481–1498.
- (21) Schweiger, A.; Jeschke, G. *Principles of Pulse Electron Paramagnetic Resonance*; Oxford University Press: Oxford, U.K., 2001.
- (22) Lakshmi, K. V.; Brudvig, G. W. *Electron Paramagnetic Resonance Distance Measurements in Photosystems*; Kluwer Academic/Plenum Publishers: New York, 2000.
- (23) Lakshmi, K. V.; Brudvig, G. W. *Curr. Opin. Struct. Biol.* **2001**, 11, 523.
- (24) Bennati, M.; Prisner, T. F. *Rep. Prog. Phys.* **2005**, 68, 411.
- (25) Mobius, K. *Appl. Magn. Reson.* **1995**, 9, 389–407.
- (26) Stehlik, D.; Mobius, K. *Annu. Rev. Phys. Chem.* **1997**, 48, 745–784.
- (27) Mobius, K.; Savitsky, A.; Schnegg, A.; Plato, M.; Fuchs, M. *Phys. Chem. Chem. Phys.* **2005**, 7, 19–42.
- (28) Schnegg, A.; Dubinskii, A. A.; Fuchs, M. R.; Grishin, Y. A.; Kirilina, E. P.; Lubitz, W.; Plato, M.; Savitsky, A.; Mobius, K. *Appl. Magn. Reson.* **2007**, 31, 59–98.
- (29) Prisner, T.; Rohrer, M.; MacMillan, F. *Annu. Rev. Phys. Chem.* **2001**, 52, 279–313.
- (30) Sinnecker, S.; Flores, M.; Lubitz, W. *Phys. Chem. Chem. Phys.* **2006**, 8, 5659–5670.
- (31) Lakshmi, K. V.; Reifler, M. J.; Brudvig, G. W.; Poluektov, O. G.; Wagner, A. M.; Thurnauer, M. C. *J. Phys. Chem. B* **2000**, 104, 10445–10448.
- (32) Savitsky, A.; Mobius, K. *Photosyn. Res.* **2009**, 102, 311–333.
- (33) Lubitz, W.; Feher, G. *Appl. Magn. Reson.* **1999**, 17, 1–48.
- (34) Levanon, H.; Mobius, K. *Annu. Rev. Biophys. Biomol. Struct.* **1997**, 26, 495.
- (35) Dorlet, P.; Rutherford, A. W.; Un, S. *Biochemistry* **2000**, 39, 7826–7834.
- (36) Kamlowski, A.; Altenberg-Greulich, B.; van der Est, A.; Zech, S. G.; Bittl, R.; Fromme, P.; Lubitz, W.; Stehlik, D. *J. Phys. Chem. B* **1998**, 102, 8278–8287.
- (37) Rohrer, M.; Gast, P.; Mobius, K.; Prisner, T. F. *Chem. Phys. Lett.* **1996**, 259, 523–530.
- (38) Rinkevicius, Z.; Telyatnyk, L.; Vahtras, O.; Ruud, K. *J. Chem. Phys.* **2004**, 121, 5051–5060.
- (39) Burghaus, O.; Plato, M.; Rohrer, M.; Mobius, K.; Macmillan, F.; Lubitz, W. *J. Phys. Chem.* **1993**, 97, 7639–7647.
- (40) Kacprzak, S.; Kaupp, M.; MacMillan, F. *J. Am. Chem. Soc.* **2006**, 128, 5659–5671.
- (41) Sinnecker, S.; Reijerse, E.; Neese, F.; Lubitz, W. *J. Am. Chem. Soc.* **2004**, 126, 3280–3290.
- (42) Asher, J. R.; Kaupp, M. *Theor. Chem. Acc.* **2008**, 119, 477–487.
- (43) Asher, J. R.; Doltsinis, N. L.; Kaupp, M. *J. Am. Chem. Soc.* **2004**, 126, 9854–9861.
- (44) Macmillan, F.; Lenzian, F.; Renger, G.; Lubitz, W. *Biochemistry* **1995**, 34, 8144–8156.
- (45) Rohrer, M.; MacMillan, F.; Prisner, T. F.; Gardiner, A. T.; Mobius, K.; Lubitz, W. *J. Phys. Chem. B* **1998**, 102, 4648–4657.
- (46) Un, S.; Dorlet, P.; Rutherford, A. W. *Appl. Magn. Reson.* **2001**, 21, 341–361.
- (47) Ciofini, I.; Reviakine, R.; Arbuznikov, A.; Kaupp, M. *Theor. Chem. Acc.* **2004**, 111, 132–140.
- (48) Nimz, O.; Lenzian, F.; Boullais, C.; Lubitz, W. *Appl. Magn. Reson.* **1998**, 14, 255–274.
- (49) Weyers, A. M.; Chatterjee, R.; Milikisoyants, S.; Lakshmi, K. V. *J. Phys. Chem. B* **2009**, 113, 15409–15418.
- (50) Lakshmi, K. V.; Reifler, M. J.; Chisholm, D. A.; Wang, J. Y.; Diner, B. A.; Brudvig, G. W. *Photosyn. Res.* **2002**, 72, 175–189.
- (51) Rippka, R.; Deruelles, J.; Waterbury, J. B.; Herdman, M.; Stanier, R. Y. *J. Gen. Microbiol.* **1979**, 111, 1–61.
- (52) Tamura, N.; Cheniae, G. *Biochim. Biophys. Acta* **1987**, 890, 179–194.
- (53) Deligiannakis, Y.; Rutherford, A. W. *Biochim. Biophys. Acta, Bioenerg.* **1998**, 1365, 354–362.
- (54) Poluektov, O. G.; Utschig, L. M.; Schlesselman, S. L.; Lakshmi, K. V.; Brudvig, G. W.; Kothe, G.; Thurnauer, M. C. *J. Phys. Chem. B* **2002**, 106, 8911–8916.
- (55) Stone, A. J. *Mol. Phys.* **1963**, 6, 509–515.
- (56) Knupling, M.; Topping, J. T.; Un, S. *Chem. Phys.* **1997**, 219, 291–304.
- (57) Kaupp, M.; Remenyi, C.; Vaara, J.; Malkina, O. L.; Malkin, V. G. *J. Am. Chem. Soc.* **2002**, 124, 2709–2722.
- (58) Prabhananda, B. S.; Felix, C. C.; Hyde, J. S.; Walvekar, A. *J. Chem. Phys.* **1985**, 83, 6121–6127.
- (59) Yonezawa, T.; Kawamura, T.; Ushio, M.; Nakao, Y. *Bull. Korean Chem. Soc.* **1970**, 43, 1022–1027.
- (60) Chatterjee, R.; Milikisoyants, S.; Coates, C. S.; Lakshmi, K. V. *Biochemistry* **2011**, 50, 491–501.
- (61) Ishikita, H.; Knapp, E. W. *J. Am. Chem. Soc.* **2005**, 127, 14714–14720.